13

The Basics of Gas Sorption and Separation in MOFs

13.1 Gas Adsorption

A certain terminology and specific theoretical models are used to describe and evaluate the properties of porous materials with respect to the storage and separation of gases. Some of these terms and models, including the Langmuir and BET theory, were already introduced in Chapter 2. In contrast to the simple evaluation of porosity when considering the application of porous materials, the following parameters gain in importance: (i) working capacity, (ii) system capacity, (iii) kinetics, (iv) cycling stability, (v) isosteric heat of adsorption (Q_{st}), and (vi) selectivity. There are cases where additional differentiation between the excess and total uptake, and the gravimetric and volumetric uptake is helpful. In this chapter, we present definitions and physical principles underlying these parameters.

13.1.1 Excess and Total Uptake

When dealing with gas storage it is important to differentiate between the excess and the total uptake of a given material. Most gas adsorption experiments are carried out between ambient pressure and a pressure of approximately 1 bar. In this regime, the excess and total adsorption values are almost identical. For the adsorption of gases at high pressures (>5 bar), a pressure regime that is of interest for automotive applications, it is instructive to perform high pressure adsorption measurements to simulate application conditions. At high pressures, the excess and total uptake can differ considerably (Figure 13.1). The difference in gas uptake between two containers, one of them filled with a porous adsorbent and the other one being empty and of the same volume as the total pore volume of the porous framework (adsorbent), is referred to as the excess adsorption, also known as Gibbs excess. This quantity is correlated to the adsorption of gas molecules on the inner pore surface of the porous material. The excess adsorption reaches a maximum at elevated pressures (generally between 20 and 40 bar) and subsequently decreases again. This is attributed to the lower efficiency of packing and compressing of gas molecules within the pores of the adsorbent in this pressure range compared to a free volume (e.g. empty gas cylinder).

Introduction to Reticular Chemistry: Metal-Organic Frameworks and Covalent Organic Frameworks,
First Edition. Omar M. Yaghi, Markus J. Kalmutzki, and Christian S. Diercks.

Companion website: www.wiley.com/go/yaghi/reticular

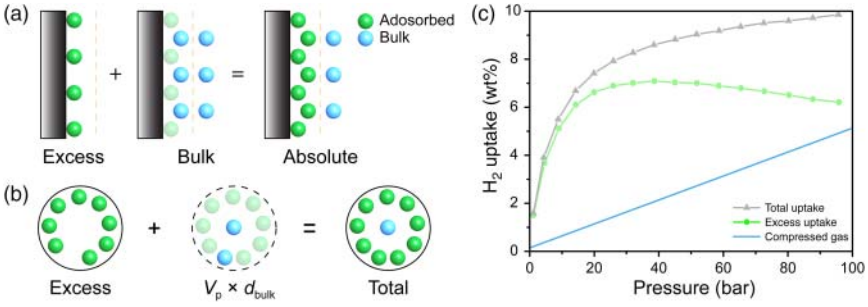

Figure 13.1 (a) Adsorption on a two-dimensional surface: the Gibbs dividing surface (light orange) divides the free volume into adsorbed (green) and bulk (blue) gas molecules [1]. The bulk gas molecules are the molecules that would be present in the pore volume in the absence of adsorption (middle). The absolute adsorption includes all gas molecules in the adsorbed state, meaning the sum of the experimentally measured excess adsorption and the bulk gas molecules (right). (b) The total adsorption in the pores of a porous framework material consists of all gas molecules inside the total pore volume (the sum of the excess adsorption and the bulk gas) [2]. The total adsorption is often used as an approximation for absolute adsorption in microporous materials, since experimental determination of the Gibbs dividing surface of microporous materials is not possible. (c) High-pressure H_2 adsorption measurement on MOF-5 with the total (gray triangles) and excess uptake (green circles) as well as the uptake of a gas cylinder (blue line) representing the bulk gas uptake.

Measurements at pressures beyond the maximum of the excess adsorption are necessary to estimate the total uptake of a material. At high pressures the total amount of gas molecules per volume of adsorbent consists of adsorbed molecules and compressed bulk gas in the pores that does not interact with the surface of the pores. The total uptake includes both the gas molecules adsorbed on the surface and those compressed within the pores of the framework and is described by Eq. (13.1):

$$N_{\text{tot}} = N_{\text{ex}} + d_{\text{gas}} V_{\text{pore}} \tag{13.1}$$

where N_{tot} is the total uptake in mg g^{-1}, N_{ex} is the excess uptake in mg g^{-1}, d_{gas} is the density of the gas at a given pressure in mg cm^{-3}, and V_{pore} is the pore volume in cm^3 g^{-1}. The pore volume is calculated from the crystallographic density (d_{cryst} in g cm^{-3}) and the skeletal density (d_{skeletal} in g cm^{-3}, determined by pycnometry) according to Eq. (13.2) or is calculated from gas sorption isotherms.

$$V_{\text{pore}} = \frac{1}{d_{\text{cryst}}} - \frac{1}{d_{\text{skeletal}}} \tag{13.2}$$

For materials with small pores (micropores) the second term in Eq. (13.1) ($d_{\text{gas}} V_{\text{pore}}$) becomes very small since the free pore volume after (a monolayer of) gas is adsorbed on the surface becomes very small. Consequently, the total uptake for microporous materials is often overestimated. Knowledge of the total uptake facilitates the determination of the volumetric storage density, one of the most important quantities with respect to gas storage in energy applications. As discussed earlier, these fundamental properties do not account for the efficiency of packing in a container. This is however of importance for the overall efficiency

of a storage system. Both the excess and total gas uptake are commonly provided in units of weight percentage (wt%) calculated according to Eq. (13.3).

$$\text{wt\%} = \frac{(m_{\text{adsorbate}})}{(m_{\text{adsorbent}} + m_{\text{adsorbate}})} \cdot 100\% \tag{13.3}$$

Since the second term in the denominator is often neglected, leading to overestimated wt% values, it is recommended to use the unit $\text{g}\,\text{g}^{-1}$ (mass of gas adsorbed per mass of adsorbent) when comparing the uptake of different materials to ensure comparability.

13.1.2 Volumetric Versus Gravimetric Uptake

Owing to their open structures, metal-organic frameworks (MOFs) often have low densities, which is expected to result in high values for the gravimetric gas uptake ($\text{cm}^3\ \text{g}^{-1}$ or $\text{g}\,\text{g}^{-1}$). A high gravimetric uptake however acts against achieving a high volumetric uptake ($\text{cm}^3\ \text{cm}^{-3}$ or $\text{g}\,\text{cm}^{-3}$). To understand this, we consider a gas that is compressed within a porous material with large open pores. In this scenario, a large fraction of this gas, although floating in the pores, does not interact with the internal surface and therefore behaves like compressed gas in a gas cylinder. In other words, there is no advantage gained by having gas compressed in the pores of such material since gas molecules interacting with the framework are packed more closely than gas molecules that are compressed within the pores at high pressures. Therefore, we expect a high gravimetric uptake but a low volumetric storage capacity for such low-density materials with large pore diameters. This is especially pronounced for covalent organic frameworks (COFs) owing to their ultralow density. In conclusion, this means that a balance must be struck between the size of the pores (gravimetric uptake) and having high volumetric uptake, especially when considering applications such as energy storage in mobile devices where a low volumetric uptake is highly unfavorable. This balance is attained by adjusting the pore diameter and/or the strength of the interaction with the adsorbate, both parameters that are different for different gas species. This point is elaborated further in the respective chapters.

13.1.3 Working Capacity

The maximum gas uptake measured by gas adsorption experiments is a useful quantity for the evaluation of porous materials; however, it does not represent the usable capacity under application conditions. For illustrative purposes, we consider a device powered by a gaseous fuel that requires a minimum delivery pressure to function (typically $P_{\text{min}} = 5\,\text{bar}$). Additionally, a reasonable upper pressure limit must be chosen. In general, the upper limits are $P_{\text{max}} = 35$ or 65 bar, which correspond to the limits of single- and dual-stage compressors, respectively [3]. These prerequisites lower the accessible capacity in comparison to the maximum uptake determined by gas adsorption measurements and the corresponding uptake is therefore commonly referred to as the "working capacity" (Figure 13.2). The working capacity gives the amount of gas that can be delivered to the device when the pressure is lowered from the maximum pressure of the

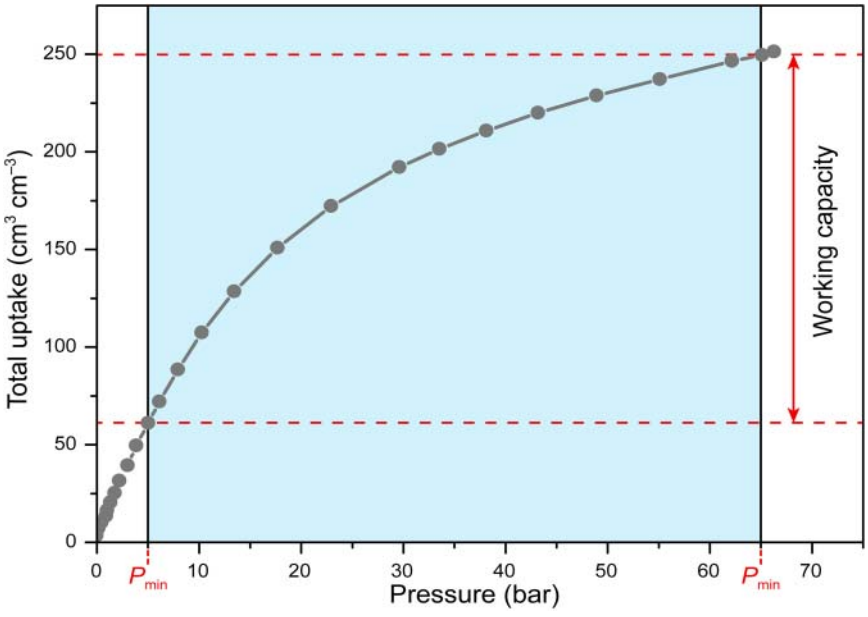

Figure 13.2 An example of a methane isotherm between 0 and 65 bar recorded at room temperature [4]. The working capacity is the deliverable amount of gas between 65 and 5 bar under isothermal conditions and is in this example about 60 cm^3 cm^{-3} lower than the total uptake. The pressure limits are chosen based on the maximum pressure of a dual-stage compressor and the minimum inlet pressure of a methane-powered combustion engine.

tank to the minimum inlet pressure of the device. With respect to applications, depending on the adsorption and desorption behavior of the material, the total uptake in wt% is not accessible and to estimate the working capacity the uptake at low (<5 bar) and high pressures (>35 or 65 bar) must be excluded.

13.1.4 System-Based Capacity

To estimate the deliverable capacity of gas storage materials on the system level, factors such as the weight and volume of all auxiliary system components including items such as the storage vessel, the working capacity, thermal and pressure management equipment, valves, piping, and sensors need to be considered.

Intrinsic thermal effects in the gas storage system have a dramatic impact on the storage capacity. The heat released upon refueling (Q_{st}) must be dissipated efficiently; otherwise, the adsorbent bed heats up, which results in a lower gas storage capacity. By the same token, if the thermal energy that is consumed during the discharge process is not resupplied, the temperature of the adsorbent bed drops, resulting in the retention of a large amount of gas at low pressure. Therefore, the absolute capacity on a system level of any given porous gas storage material is always lower than its working capacity determined by gas adsorption experiments. The system-based capacity provides an upper limit to the amount of usable gas in a device (Figure 13.3).

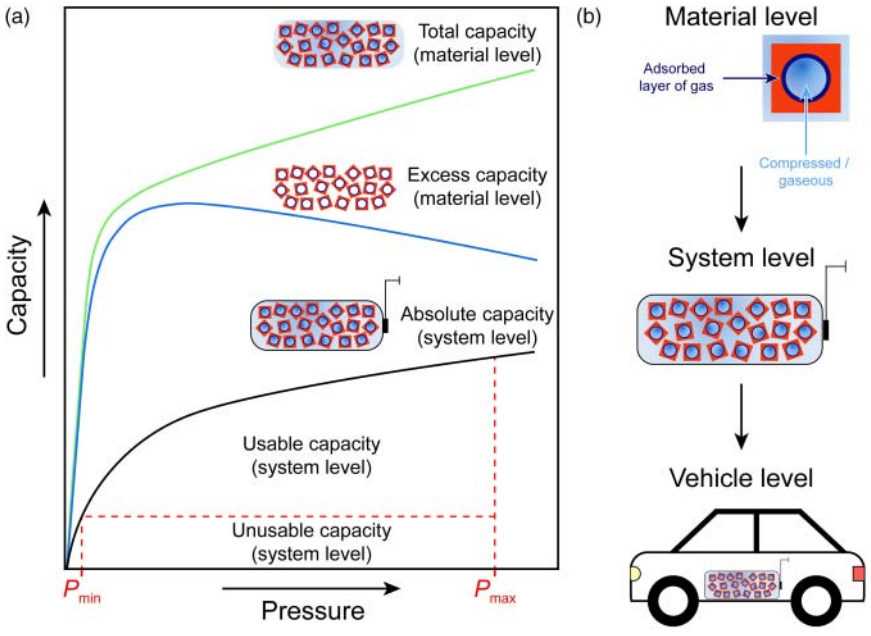

Figure 13.3 (a) Schematic isotherms representing the total (green line), excess (blue line), and absolute (black line) methane storage capacity of a porous adsorbent. Since here the weight of the storage vessel is considered, the gravimetric capacity on the system level is drastically decreased compared to the maximum uptake determined by gas adsorption measurements. The usable capacity is determined by excluding the uptake outside the pressure limits given by the compressor system (upper boundary, P_{max}) and the minimum operating pressure (lower boundary, P_{min}). (b) On the material level the total and excess capacity are distinguished, whereas the system-based capacity is calculated from the total capacity considering the weight of the storage vessel. At the vehicle level, additional factors such as intrinsic thermal effects must be considered.

13.2 Gas Separation

Separation of gases in porous solids follows either a thermodynamic or a kinetic separation mechanism. The separation of gaseous mixtures based on physisorption or chemisorption of the adsorbate to specific adsorption sites within the porous solid is a thermodynamic process and is hence termed "thermodynamic separation." A gaseous mixture can also be separated if the individual components diffuse with different diffusivities or follow different diffusion pathways, a process termed "kinetic separation." Often, both mechanisms are present simultaneously and it is important to understand which of them is rate limiting. The next section will give an insight into the different mechanisms of gas diffusion in porous solids and their importance with respect to gas separation.

13.2.1 Thermodynamic Separation

Thermodynamic or equilibrium separation is found for materials with pore apertures that are large enough to allow for all adsorbate molecules to pass

unhindered ($d_{pore} \gg d_{kinetic(gas)}$). For this case, the separation is governed by the differences between the affinities of the individual components of the mixture toward the surface of the adsorbent. Thus, the selectivity can be tuned by introducing specific functionalities or binding sites to modulate the strength of the interaction between a specific component of the mixture and the inner pore surface. The isosteric heat of adsorption (Q_{st}) at zero coverage correlates with the magnitude of the strongest interaction between the adsorbate and the adsorbent, making Q_{st} a significant quantity in the design of porous materials for gas storage and separation. Chemical modifications carried out on a framework material such as covalent modifications, introduction of functional groups, and the creation of open metal sites (see Chapter 6) may result in a change in the Q_{st} value and consequently such modifications are used as a handle for optimizing the thermodynamics of the adsorption process. Q_{st} can be calculated from adsorption isotherms recorded at two different temperatures (typically 77 and 87 K) by fitting the data to either the virial (see Section 13.2.1.1) or the Langmuir–Freundlich equation (see Section 13.2.1.2).

13.2.1.1 Calculation of Q_{st} Using a Virial-Type Equation

The following virial-type equation is used to fit the adsorption data at a given fixed temperature following Eq. (13.4):

$$\ln(N/P) = A_0 + A_1N + A_2N^2 + A_3N^3 + \cdots \tag{13.4}$$

where P is the pressure, N is the amount of gas adsorbed, and A_0, A_1, etc. are the virial coefficients. Q_{st} is calculated as a function of coverage using the Clausius–Clapeyron equation.

$$Q_{st} = R \ln\left(\frac{P_1}{P_2}\right)\frac{T_1T_2}{T_2 - T_1} \tag{13.5}$$

The virial analysis is mathematically consistent since it can be reduced to Henry's law and allows to estimate the Q_{st} at zero coverage by extrapolation. For higher values of coverage, it shows only minimal deviations for all experimental data points; however, the use of polynomials of too high order can result in an overinterpretation.

13.2.1.2 Calculation of Q_{st} Using the Langmuir–Freundlich Equation

The Langmuir–Freundlich equation can be used to fit adsorption data at a fixed temperature following Eq. (13.6):

$$\frac{N}{N_m} = \frac{BP^{(1/t)}}{1 + BP^{(1/t)}} \tag{13.6}$$

where P is the pressure, N is the amount of gas adsorbed, and B and t are constants. Eq. (13.6) can be rearranged to yield an expression for P (Eq. (13.7)) that allows for the determination of Q_{st} using the Clausius–Clapeyron equation (Eq. (13.5)).

$$P = \left(\frac{N/N_m}{B + BN/N_3}\right) \tag{13.7}$$

13.2.2 Kinetic Separation

Kinetic or nonequilibrium gas separation mechanisms are based on the differences in the diffusion behavior of gases. In general, molecules with high mobility permeate the pore space more quickly than molecules of lower mobility. The diffusivity of a given gas can be influenced by adjustment of the pore metrics and the dimensionality of the pore system. Subtle changes in the pore structure of a porous solid can result in a significant change in the diffusivity of a specific type of molecule by an order of magnitude. In a similar way, structural changes of the diffusing species (e.g. *iso*- and *n*-alkanes) can have a dramatic influence.

13.2.2.1 Diffusion Mechanisms

When considering transport processes of gases within porous solids one must distinguish between convection (transport of gases due to a pressure gradient) and diffusion (transport of gases due to a concentration gradient). In this chapter, we will only consider diffusion mechanisms since diffusion is easily distinguished from convective flow and is the main mechanism in the kinetic separation of gases. Which diffusion mechanism predominates depends on the ratio of the pore diameter and the mean free path of the gas molecules. Within the large free space between particles "normal diffusion" as we are familiar with from gaseous mixtures dominates. Confined pores of a diameter significantly larger than the kinetic diameter of the diffusing gas molecules lead to a transition from normal diffusion to "molecular diffusion." Decreasing the pore size to the regime of the mean free path of the gas molecules leads to "Knudsen diffusion" and for the case of even smaller pore sizes, in the same regime as the kinetic diameter of the gas molecules, "configurational diffusion" is prevalent. Figure 13.4a gives a correlation between the pore size and the mechanism of diffusion. In addition to the mechanisms mentioned above, molecules always undergo adsorption on the surface and move along the surface in a process termed "surface diffusion." We can describe the interplay of the different mechanisms of diffusion analogous to an electric circuit. Molecular and Knudsen diffusion act like resistors in a series circuit, whereas surface diffusion and convective flow are described by resistors wired parallel to molecular and Knudsen diffusion (Figure 13.4b).

Molecular Diffusion Molecular diffusion occurs in porous solids with pores significantly larger than the kinetic diameter of the gas molecules diffusing through the solid. In the absence of a bulk flow (i.e. convection), the steady-state molar flux (j_A) in the z-direction is described by Fick's law:

$$j_A = -D_A \frac{dc_A}{dz} \tag{13.8}$$

where D_A is the diffusivity of the component A through the porous solid and c_A is its concentration. The diffusion through a slab of material of thickness z is determined by integration of Eq. (13.8) based on the assumption of a linear concentration gradient, which leads to Eq. (13.9).

$$j_A = \frac{D_A (c_{A1} - c_{A2})}{z} \tag{13.9}$$

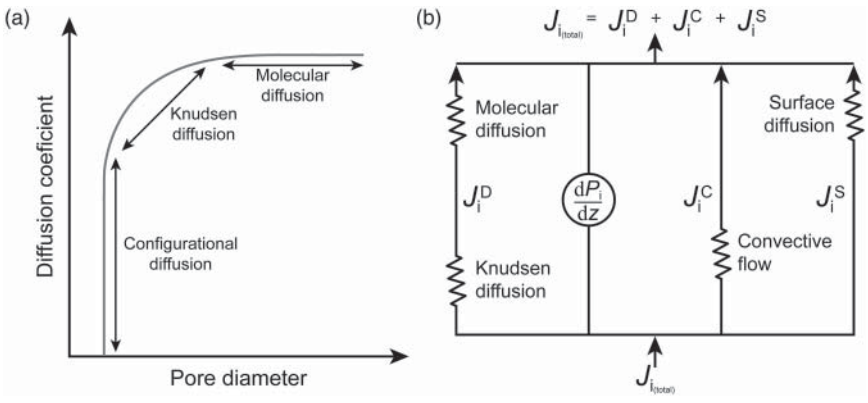

Figure 13.4 (a) Correlation between pore size and diffusion mechanism. For pores that are significantly larger than the kinetic diameter of the diffusing gas molecules, molecular diffusion is observed. From a mechanistic point of view, molecular diffusion is similar to normal diffusion since molecule–molecule collisions are more likely to occur than molecule–pore collisions. For pores in the regime of the mean free path of the gas molecules, Knudsen diffusion is the predominant mechanism and for even smaller pores in the regime of the kinetic diameter of the gas molecules configurational diffusion is observed. (b) Different diffusion mechanisms can be described analogous to an electric circuit where the different types of diffusion are represented by resistors. Molecular and Knudsen diffusion can be described by resistors in a series circuit (flux J_i^D), whereas surface diffusion (flux J_i^S) and convective flow (flux J_i^C) are represented by resistors wired parallel to molecular and Knudsen diffusion.

Here, c_{A1} and c_{A2} are the concentrations of component A at z_1 and z_2, the two opposite sides of the slab of thickness z, respectively. For solids of different shapes, the rate of diffusion (w) is described by Eq. (13.10):

$$w = j_A S_{av} = \frac{D_A S_{av}(c_{A1} - c_{A2})}{z} \tag{13.10}$$

where S_{av} is the average cross section for diffusion through a slab of a porous material of thickness z. This assumption holds true for perfect crystals with uniform pores of a diameter significantly larger than the mean free path of the diffusing gas molecules and of equal length z. Owing to the comparatively large size of the pore compared to the mean free path of the gas molecules the resistance is mainly due to molecule–molecule collisions, and the probability for molecule–pore wall collisions to occur is comparatively low. This, however, changes when the pore diameter is decreased, resulting in diffusion following a different mechanism: Knudsen diffusion.

Knudsen Diffusion Knudsen diffusion is predominant in materials with pore sizes in the regime of the mean free path of the diffusing gas molecules. Owing to the smaller pores, molecule–pore wall collisions dominate over molecule–molecule collisions. Knudsen diffusion is observed for "thin gases" (i.e. low probability of

molecule–molecule collisions) in porous solids. The Knudsen diffusivity (D_K in $s^{-1}\,cm^{-2}$) of a gas in a cylindrical pore is given by Eq. (13.11):

$$D_{K,\,pore} = \frac{2}{3} r \sqrt{\frac{8}{\pi} \cdot \frac{RT}{M}} \tag{13.11}$$

where r is the pore radius, M is the molar mass of the gas diffusing in the pore, and $^2/_3$ accounts for the cylindrical shape of the pore. Since the presence of exclusively cylindrical pores in a porous solid is relatively rare, an equation allowing for the calculation of the diffusivity in porous materials with more complex pore systems is needed (Eq. (13.12)).

$$D_{K,\,porous\,medium} = D_{K,\,pore} \frac{\varepsilon \cdot \delta}{\tau} \tag{13.12}$$

Here, ε is the porosity (i.e. overall porosity minus pores that are too small for the gas to enter and impasses), δ is the constrictivity (i.e. the deceleration of diffusion due to an increase in viscosity in narrow pores), and τ is the tortuosity (i.e. intricacy), which compensates for the deviation of the pore structure from an array of parallel cylindrical pores.

By decreasing the size of the pores further until a value close to the diameter of the gas molecule is reached, a transition into configurational diffusion occurs. This type of diffusion can only be described with sophisticated models, and for further explanations the reader is referred elsewhere [5].

Surface Diffusion Surface diffusion is an activated process and is strongly correlated to the adsorption–desorption equilibrium on the inner surface of the porous material. This means that the potential on the surface of the adsorbent is not flat and an activation barrier has to be overcome for surface diffusion to occur. Surface diffusion can proceed following two mechanisms:

(i) If the activation energy (E_{diff}) for diffusion is lower than the thermal energy (i.e. kT) molecules diffuse "freely" on the surface, which is typically the case for physisorption.
(ii) If E_{diff} is higher than kT, molecules move following a hopping mechanism typically observed for chemisorbed species. Hopping can occur over long distances since a molecule that has reached the energetically high transition state can migrate along multiple adsorption sites before it has dissipated enough energy to be re-adsorbed on the surface.

13.2.2.2 Influence of the Pore Shape

It can be readily recognized that the metrics of the pores in a porous solid have an impact on the diffusivity since they determine the predominant diffusion mechanisms. However, the shape of the pores is just as important. Differently shaped pores of the same diameter result in significantly different diffusivities. Generally, cylindrical pores allow for the highest diffusivity since both the constrictivity (δ) and tortuosity (τ) can be neglected. Figure 13.5 shows a comparison of the time

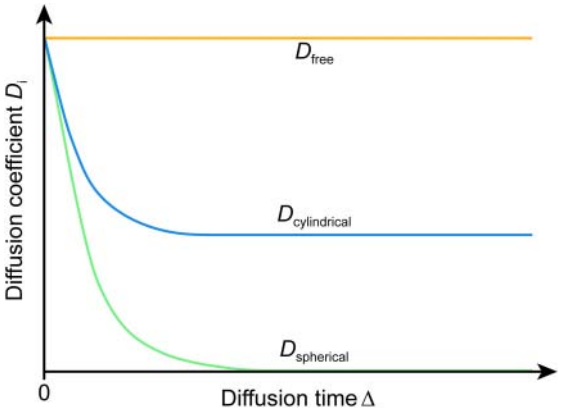

Figure 13.5 Dependence of the diffusion coefficient D_i on the diffusion time Δ. For normal diffusion, the diffusion coefficient (D_{free}) is independent of Δ (orange line). For cylindrical pores, the diffusion is hindered and therefore $D_{cyl.}$ decreases and reaches a lower limit for $\Delta \rightarrow \infty$ (blue line). In closed spherical pores $D_{sph.}$ decreases proportional to Δ^2 and reaches zero for $\Delta \rightarrow \infty$ (green line). The diffusion coefficient for spherical pores connected through narrow windows shows a dependence on Δ similar to that of cylindrical pores; however, in general a lower value of D is expected for $\Delta \rightarrow \infty$. The corresponding graph for 3D pore systems would be situated in the area between that of cylindrical and spherical pores.

dependence of the diffusion coefficient for different pore shapes. At $t = t_0$ the diffusion coefficients of the free gas (D_{free}), and the cylindrical (D_{cyl}) and spherical pores (D_{sph}) are identical. D_{free} is constant whereas D_{cyl} decreases due to an increase in resistance (e.g. increase in viscosity), and D_{sph} eventually approaches zero after clogging of the spherical pores. Diffusion coefficients of 3D pore systems (D_{3D}) containing cages connected through narrow windows show a similar trend to that of spherical pores; however, D_{3D} does not approach zero and the diffusion coefficient reached at $\Delta \rightarrow \infty$ depends on the diameter of the pore windows.

13.2.2.3 Separation by Size Exclusion

Separation by size-selective exclusion is found in materials with narrow pores that are smaller than the kinetic diameter of at least one component in a mixture. This means that at least one gas species cannot enter the pore system due to steric hindrance while others with a smaller kinetic diameter can. This type of separation is often undesirable since it is accompanied by a dramatic pressure drop. Therefore, larger pore sizes and a transition from molecular sieving to kinetic separation or partial molecular sieving are more appealing.

13.2.2.4 Separation Based on the Gate-Opening Effect

The gate-opening effect denotes a process associated with a structural transition from a narrow pore (*np*) phase of low porosity to a wide pore (*wp*) porous phase. This effect has been proved useful for many separation processes such as C_1–C_5 separation (see Chapter 16) [6]. The gate-opening effect is often induced by temperature and/or pressure and the uptake and release of individual molecules

is controlled by these parameters, for example, by a specific threshold pressure. Owing to the spontaneous release of gas upon gate closing, a large working capacity can be achieved. This type of flexibility is exclusive to reticular materials (MOFs, COFs, and zeolitic imidazolate frameworks (ZIFs)); however, it has thus far not been possible to target such materials by design.

13.2.3 Selectivity

In separation processes the selectivity of the adsorbent toward a specific component in a gas mixture is essential. Such selectivity can be achieved through adjustment of the strength of the adsorption interactions (thermodynamic separation) or by size discrimination and differences in the diffusivities of the individual components in the mixture (kinetic separation). As we saw earlier, thermodynamic separation relies on the fact that different gases have different affinities toward the adsorption sites. Since the gas diffusion in porous solids with sufficiently large pores is unrestricted, the diffusivities of all components in the gas mixture are approximately the same and the equilibrium gas adsorption selectivity is consequently calculated from the ratio of the Henry's constants (K_i, slope of the isotherm at low relative pressures $P/P_0 \rightarrow 0$) of the individual components as in Eq. (13.13).

$$S = \frac{K_1}{K_2} \tag{13.13}$$

Thermodynamic selectivity is based on either a physisorption or chemisorption mechanism and is thus correlated to the difference in physical properties of the various gases in the mixture (e.g. polarizability, quadrupole moment) that influence the isosteric heat of adsorption. To illustrate this, we consider a mixture of CO_2 (15–16%) and N_2 (73–77%), a composition similar to that of post-combustion flue gas. A comparison of the physical parameters relevant for their equilibrium separation reveals that both the polarizability (CO_2, 29.1×10^{-25} cm^{-3}; N_2, 17.4×10^{-25} cm^{-3}) and quadrupole moment (CO_2, 4.3×10^{26} esu^{-1} cm^{-2}; N_2, 1.52×10^{26} esu^{-1} cm^{-2}) of CO_2 are higher than those of N_2. Polar sites located on the pore surface of the capture material will therefore lead to a stronger interaction with and a higher affinity/selectivity for CO_2.

Kinetic separation presupposes a size selectivity caused by appropriately sized pores. A porous material with small pores only permits molecules up to a certain kinetic diameter to diffuse freely, whereas larger molecules will not be able to permeate the capture material due to spatial limitations resulting in nonequilibrium separation [7]. For MOFs with small pores that reach the kinetic diameter of the gas components, the diffusion of these gases becomes increasingly difficult. We saw earlier that in this case the molecular diffusion will gradually evolve into Knudsen or even surface diffusion, thus rendering the diffusivities of the gas components distinguishable. Since surface diffusion is always present, the kinetic separation factor is defined by both the ratio of the Henry's constants (K_i) and the ratio of the diffusivities (D_i) (Eq. (13.14)) [8].

$$S = \frac{K_1}{K_2} \cdot \sqrt{\frac{D_1}{D_2}} \tag{13.14}$$

This kinetic effect may sometimes enhance the equilibrium adsorption selectivity but is more often found to decrease the selectivity, especially if the more strongly adsorbing component diffuses much slower than the less strongly adsorbing component [9]. Kinetic separation is only applicable to mixtures of gases with significantly different kinetic diameters. The previous example of a CO_2/N_2 mixture used to illustrate the thermodynamic selectivity does not fulfill this prerequisite since both molecules have a similar kinetic diameter (3.68 and 3.30 Å, respectively). This would require the pore openings of the capture material to be very small and within a narrow range. Small pore diameters however limit the diffusion of gases throughout the material and additionally the presence of defects (which cannot be avoided) results in larger pores sizes, thus rendering this approach less viable (Figure 13.6b). In contrast, as depicted in Figure 13.6a, a mixture of differently sized gases such as *trans*-butylene and *iso*-butylene fulfills this prerequisite.

Three ways are commonly used to determine the selectivity of a given porous material from experimental data: (i) estimation from single-component isotherms, (ii) calculation following the ideal adsorbed solution theory (IAST), and (iii) from breakthrough experiments.

13.2.3.1 Calculation of the Selectivity from Single-Component Isotherms

To calculate a "selectivity factor" the experimental isotherms for the two gases in question need to be known. It is calculated following Eq. (13.15):

$$S = \frac{q_1/q_2}{P_1/P_2} \tag{13.15}$$

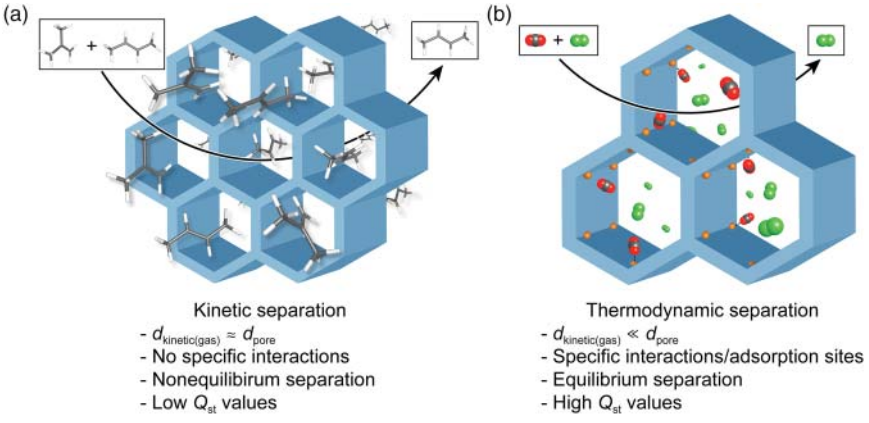

Figure 13.6 Kinetic and thermodynamic separation in porous materials. (a) Kinetic separation relies on different diffusivities of the components of the influent gas mixture. *trans*-Butylene and *iso*-butylene have different kinetic diameters; therefore, only the linear *trans*-butylene can permeate through the pores, whereas *iso*-butylene is held back. (b) Thermodynamic separation relies on specific interactions with one component of the influent gas mixture. CO_2 is bound strongly to specific adsorption sites, whereas N_2 can diffuse through the pores unhindered.

where the selectivity factor S is given as the molar ratio of the adsorbed quantities (q_i) and the partial pressures (P_i) of the gases. Since this estimation originates from single-component adsorption isotherms it does not consider that different types of gas molecules can compete for the same adsorption site. Even though the selectivity factors calculated using this method are not accurate, it allows for the facile qualitative evaluation of different porous adsorbents.

13.2.3.2 Calculation of the Selectivity by Ideal Adsorbed Solution Theory

A more accurate calculation of the selectivity from single-component isotherms is realized when the IAST is used [10]. The IAST is a viable method for gas mixtures where both components mix and behave as ideal gases. To calculate the selectivity following the IAST, isotherms of the single components of the gas mixture must be measured at the same temperature and fitted using mathematical methods. The mole fraction of each species in the adsorbed phase is then calculated by solving the integrals for the single components given by Eq. (13.16):

$$\int_0^{P\cdot y_i/x_i} \frac{\text{Isotherm for component } i(P)}{P} dP = \int_0^{P\cdot y_j/x_j} \frac{\text{Isotherm for component } j(p)}{P} dP \tag{13.16}$$

where P is the total pressure, x_i/x_j are the mole fractions of the adsorbed gas, and y_i/y_j those of the bulk phase of components i and j, respectively. The accuracy of this theory is reduced for high mixture fractions of the less adsorbed component since it requires the integration of the single-component isotherm up to extremely high pressures. The gas adsorption in flexible frameworks is not described accurately by the IAST but other methods applicable to such solids have been developed [11]. The amount of adsorbed gas in the mixture is determined following Eq. (13.17), with n_{tot} being the total number of moles adsorbed in the mixture at a given pressure and n_i^0/n_j^0 the amount of the pure components i and j per gram of adsorbent.

$$\frac{1}{n_{tot}} = \frac{x_i}{n_i^0} + \frac{x_j}{n_j^0} \tag{13.17}$$

High-quality single-component data are required for accurate simulations using the IAST. It is often advantageous to use isotherms calculated using grand canonical Monte Carlo (GCMC) methods to allow for a better fit, and therefore supporting GCMC simulations are often reported alongside IAST calculations [12]. Both methods have their limitations and it is important to evaluate and scrutinize the selectivity factors calculated with them. The IAST underestimates the CO_2/H_2 selectivity for HKUST-1, which is attributed to the presence of differently shaped and sized pockets within its structure. Such pockets give rise to preferred adsorption of one gas over the other due to their difference in size. This issue is circumvented by substantiating the results gained from the IAST with GCMC simulations. Similarly, selectivity factors calculated for the separation of CO_2 and H_2 in MOF-177 using the IAST do not match

the measured data; however, a combination of GCMC and IAST predicts the selectivity in this separation accurately [13].

13.2.3.3 Experimental Methods

Breakthrough experiments give an experimental insight into the selectivity of adsorbents and allow for the experimental evaluation of their performance. In a typical setup, a defined gas mixture that is controlled by a set of mass flow controllers is fed to a measurement cell filled with powder, pellets, or a membrane containing the adsorbent. The eluent gas stream is monitored by mass spectrometry (i.e. MS or GCMS) or a set of specific gas sensors. The result of a typical measurement is depicted in Figure 13.7 where the separation of a 80 : 20 mixture of gases A and B is shown. When the gas mixture is fed to the activated adsorbent, component B is adsorbed selectively due to the lower affinity of the framework toward A, and the eluent gas stream is virtually of the pure component A. As soon as the adsorbent is saturated with B the breakthrough occurs, and the eluent gas is a mixture of A and B of varying composition until it eventually has the same composition as the influent gas mixture (A:B = 80 : 20). The adsorbent bed can subsequently be regenerated to measure multiple cycles. Regeneration

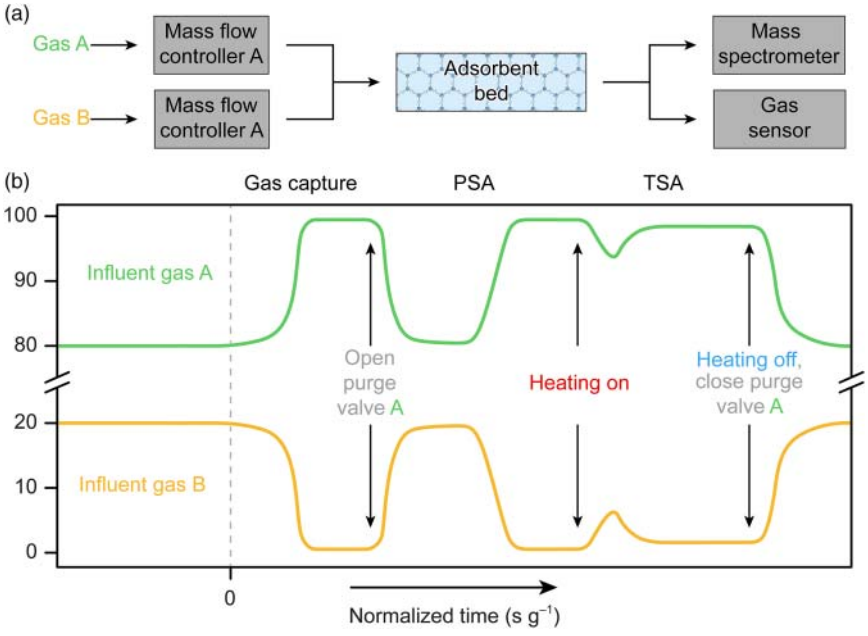

Figure 13.7 (a) Schematic of a typical breakthrough setup. Mass flow controllers are used to prepare a gas mixture with a defined composition. This mixture is fed to the adsorbent bed, which adsorbs selectively one component of the mixture. The eluent gas mixture is analyzed by mass spectrometry or specific gas sensors. Referencing the acquired data and subtraction of the dead time affords a graph similar to that shown in (b). (b) After the gas mixture is fed to the adsorbent one component is adsorbed (here, component B) until the adsorbent is saturated. The adsorbent bed is purged with component A forcing the desorption of B in a pressure swing adsorption cycle (PSA). Heating the adsorbent in a temperature swing adsorption cycle (TSA) liberates the remaining strongly bound component B, thus regenerating the adsorbent bed for another capture cycle.

is commonly realized by purging (in this example with gas A), also called "pressure swing," and subsequent heating ("temperature swing"). More details on temperature and pressure swing adsorption (PSA) are discussed in Chapter 14.

13.3 Stability of Porous Frameworks Under Application Conditions

For porous frameworks to be suitable for applications such as gas storage or separation it is inevitable for them to possess high capacities and fast kinetics. Another important factor that is often neglected is the long-term and cycling stability under application conditions. Depending on the application in question, a different set of testing conditions is required to determine the cycling stability, and these will be discussed in more detail in the chapters focusing on these applications. Even though long-term cycling studies are not necessary at the earlier stages of materials development, it is important to evaluate degradation and the associated loss in storage capacity and/or selectivity of a given material at conditions simulating those of the targeted application. Typically, this is done at a fraction of the targeted number of adsorption–desorption cycles or operating hours. Still, the insight gained from these experiments provides information for the down-selection and optimization of promising materials.

Additionally, thermal and mechanical stress can play an important role. Thermal stress occurs due to adsorption and desorption as these processes release or consume the heat of adsorption (Q_{st}), respectively. We will demonstrate the importance of thermal stability for HKUST-1 when used as a methane storage material in an automotive application. In such applications, a typical storage capacity is 20 kg of CH_4 (approximately 1250 mol or 28 000 l when considering CH_4 to be an ideal gas). The storage capacity of HKUST-1 is 0.15 g g^{-1} and therefore a tank filled with about 140 kg of HKUST-1 is required to store 20 kg of methane. The heat of CH_4 adsorption in HKUST-1 is $Q_{st} = 20\,\mathrm{kJ\,mol^{-1}}$, equaling $Q = 25\,000$ kJ of thermal energy released upon fueling, and consumed upon depletion of the tank. Plugging these numbers and the heat capacity ($c_p = 1.46\,\mathrm{kJ\,kg^{-1}\,K^{-1}}$) reported for HKUST-1 into Eq. (13.18), we can estimate an increase in temperature of more than 120 °C upon fueling [14]. This highlights the importance of testing the thermal stability of materials for gas storage applications.

$$\Delta T = \frac{Q}{m \cdot c_p} \tag{13.18}$$

Mechanical stress poses another challenge to the applicability of porous materials. Most applications do not rely on adsorbents in powder form but more commonly shaped bodies are employed. These are typically prepared by pressing or extrusion; hence the material to be processed must be mechanically stable to withstand these shaping processes without collapse of the framework structure [15]. The resulting shaped bodies need to maintain structural integrity for a long time. This gains special importance when considering mobile applications, where the material is exposed to rattling and shaking, which poses an even higher demand on the structural stability of the shaped bodies and the adsorbent alike.

13.4 Summary

In this chapter, we introduced specific terms and theories of gas adsorption and separation used with respect to the application of porous materials in gas storage and gas separation processes. We showed that for specific applications it is important to differentiate between the total and excess, and volumetric and gravimetric uptake, and that the working capacity and system-based capacity gain importance. Different diffusion mechanisms and their influence on the selectivity of separation processes were discussed and we introduced both experimental and mathematical methods for the determination of the selectivity in separation processes. In the following chapters we will use these basics to elucidate the role of MOFs in applications such as CO_2 capture and sequestration (Chapter 14), H_2 and CH_4 storage (Chapter 15), separation processes (Chapter 16), and water adsorption (Chapter 17).

References

1 Gibbs, J. (1928). *The collected Works*, vol. 1. New York: Longmans.

2 (a) Sircar, S. (1999). Gibbsian surface excess for gas adsorption revisited. *Industrial and Engineering Chemistry Research* 38 (10): 3670–3682. (b) Sircar, S. (2001). Measurement of Gibbsian surface excess. *AIChE Journal* 47 (5): 1169–1176.

3 He, Y., Zhou, W., Qian, G., and Chen, B. (2014). Methane storage in metal-organic frameworks. *Chemical Society Reviews* 43 (16): 5657–5678.

4 Li, B., Wen, H.-M., Wang, H. et al. (2015). Porous metal-organic frameworks with Lewis basic nitrogen sites for high-capacity methane storage. *Energy & Environmental Science* 8 (8): 2504–2511.

5 (a) Xiao, J. and Wei, J. (1992). Diffusion mechanism of hydrocarbons in zeolites—I. Theory. *Chemical Engineering Science* 47 (5): 1123–1141. (b) Cui, X., Bustin, R.M., and Dipple, G. (2004). Selective transport of CO_2, CH_4, and N_2 in coals: insights from modeling of experimental gas adsorption data. *Fuel* 83 (3): 293–303.

6 (a) Li, L., Krishna, R., Wang, Y. et al. (2016). Exploiting the gate opening effect in a flexible MOF for selective adsorption of propyne from $C_1/C_2/C_3$ hydrocarbons. *Journal of Materials Chemistry A* 4 (3): 751–755. (b) Gücüyener, C., van den Bergh, J., Gascon, J., and Kapteijn, F. (2010). Ethane/ethene separation turned on its head: selective ethane adsorption on the metal-organic framework ZIF-7 through a gate-opening mechanism. *Journal of the American Chemical Society* 132 (50): 17704–17706.

7 Seoane, B., Castellanos, S., Dikhtiarenko, A. et al. (2016). Multi-scale crystal engineering of metal organic frameworks. *Coordination Chemistry Reviews* 307: 147–187.

8 Do, D.D. (1998). *Adsorption Analysis: Equilibria and Kinetics: (With CD Containing Computer Matlab Programs)*, vol. 2. World Scientific.

9 (a) Nugent, P., Belmabkhout, Y., Burd, S.D. et al. (2013). Porous materials with optimal adsorption thermodynamics and kinetics for CO_2 separation. *Nature* 495 (7439): 80–84. (b) Li, L., Bell, J.G., Tang, S. et al. (2014). Gas storage and diffusion through nanocages and windows in porous metal-organic framework Cu_2(2,3,5,6-tetramethylbenzene-1,4-diisophthalate)$(H_2O)_2$. *Chemistry of Materials* 26 (16): 4679–4695.

10 (a) Myers, A. and Prausnitz, J.M. (1965). Thermodynamics of mixed-gas adsorption. *AIChE Journal* 11 (1): 121–127. (b) Myers, A. and Prausnitz, J. (1965). Prediction of the adsorption isotherm by the principle of corresponding states. *Chemical Engineering Science* 20 (6): 549–556.

11 (a) Coudert, F.-X., Mellot-Draznieks, C., Fuchs, A.H., and Boutin, A. (2009). Prediction of breathing and gate-opening transitions upon binary mixture adsorption in metal-organic frameworks. *Journal of the American Chemical Society* 131 (32): 11329–11331. (b) Coudert, F.-X. (2010). The osmotic framework adsorbed solution theory: predicting mixture coadsorption in flexible nanoporous materials. *Physical Chemistry Chemical Physics* 12 (36): 10904–10913.

12 Richter, E., Wilfried, S., and Myers, A.L. (1989). Effect of adsorption equation on prediction of multicomponent adsorption equilibria by the ideal adsorbed solution theory. *Chemical Engineering Science* 44 (8): 1609–1616.

13 Mason, J.A., Sumida, K., Herm, Z.R. et al. (2011). Evaluating metal-organic frameworks for post-combustion carbon dioxide capture via temperature swing adsorption. *Energy & Environmental Science* 4 (8): 3030–3040.

14 (a) Mu, B. and Walton, K.S. (2011). Thermal analysis and heat capacity study of metal-organic frameworks. *The Journal of Physical Chemistry C* 115 (46): 22748–22754. (b) Koh, H.S., Rana, M.K., Wong-Foy, A.G., and Siegel, D.J. (2015). Predicting methane storage in open-metal-site metal-organic frameworks. *The Journal of Physical Chemistry C* 119 (24): 13451–13458.

15 (a) Czaja, A.U., Trukhan, N., and Muller, U. (2009). Industrial applications of metal-organic frameworks. *Chemical Society Reviews* 38 (5): 1284–1293. (b) Czaja, A., Leung, E., Trukhan, N., and Müller, U. (2011). *Metal-Organic Frameworks*, 337–352. Wiley-VCH.